

A Framework for Integrating Spatial Uncertainty into Solid-Phase Measurement and Verification of Enhanced Weathering

Brian Rogers* and Kate Maher

Department of Earth System Science, Stanford University, Stanford, CA

E-mail: rogersdb@stanford.edu

Abstract

Reliable verification of enhanced weathering as a carbon dioxide removal strategy requires accurate quantification of feedstock dissolution in amended soils. However, spatial heterogeneity introduces significant uncertainty, particularly in sampling designs that rely on sparse sampling or repeated measurements at fixed locations. Here, we develop a probabilistic framework to evaluate how spatial uncertainty in solid-phase geochemical measurements influences the precision of feedstock dissolution estimates derived from an element-element mixing model. We first quantify how variance in soil compositions affects errors in modeled feedstock dissolution and apply distance-based sensitivity analysis to identify the measurement variance thresholds required to achieve desired uncertainty levels. Next, we simulate spatially heterogeneous soil conditions and various composite sampling configurations to identify the optimal sampling strategy likely to meet specified uncertainty criteria. Our findings underscore the necessity of accurately estimating field-scale variance in baseline soil concentrations prior to developing sampling plans. Analysis of data from existing high-density soil sampling campaigns indicates that geochemical variance is likely too high for element-element

17 mixing models to serve as effective near-term constraints on feedstock dissolution. The
18 framework presented here can be further extended to other solid- and multi-phase mea-
19 surement models for enhanced weathering verification.

20 **Keywords:** sensitivity analysis; Bayesian; carbon dioxide removal; CDR; soil-based;
21 monitoring, reporting, and verification; MRV; solid-phase

22 **Synopsis:** This study addresses the need for standardized uncertainty analysis and
23 reporting in open-system carbon dioxide removal applications.

24 Introduction

25 Open-system carbon dioxide removal (CDR) technologies, such as enhanced weathering
26 (EW), are being evaluated as potential keystone climate mitigation strategies. For EW,
27 however, accurate and cost-effective verification remains a major obstacle to assessing large-
28 scale effectiveness [1–4]. EW involves amending soils, usually agricultural, with a reactive
29 "feedstock", such as basalt or Mg-silicate, to shift the alkalinity of the system and effec-
30 tively dissolve additional CO₂ [5, 6]. Global projections [7–9] anticipate removals of 0.5-4
31 Gt CO₂/yr through EW, but only a fraction of these removals may be resolvable due to the
32 geochemical “noise” inherent in soil systems [10, 11].

33 Quantifying CDR in soil systems is complicated by spatial heterogeneity across scales —
34 from mineral surfaces to landscapes [12, 13] — that hinders attribution of the geochemical
35 changes arising from EW activities. Verifying CDR through EW involves constraining both
36 the rate of feedstock dissolution and the attendant increase in alkalinity and dissolved inor-
37 ganic carbon (DIC) fluxes to the groundwater and stream network [14, 15]. While aqueous
38 measurements are critical for constraining dissolved fluxes [*e.g.*, 16–18] and will thus consti-
39 tute a major portion of measurement and verification, complementary approaches based on
40 solid-phase mass balance [19] estimate cumulative feedstock dissolution using assumptions
41 about stoichiometry and baseline compositions to compute the net CDR [20–22]. However,

given the low initial enrichment of feedstock mass relative to native soil, confidently detecting a dissolution signal beyond a spatially heterogeneous baseline becomes a challenging problem [10], and accurately quantifying the magnitude of such signals can be even more challenging [23, 24].

A common current approach [19] to constrain feedstock dissolution relies on ratios of base cations to immobile elements in the solid phase. The resulting depletion and mixing equations (Eq. 1-2; Supp. 1) require analysis of multiple soil samples in sequence, from soil (baseline) to the initial mixture (soil + feedstock) to weathered compositions over multiple time points [19, 25]. These measurements are used to estimate the true fraction of feedstock dissolved (f_d), calculated as

$$f_d = 1 - \frac{[M]_{mix} - [M]_{bsln}}{[M]_{mix}^0 - [M]_{bsln}} \quad (1)$$

where $[M]$ is base cation concentration of the baseline ($bsln$), initial mixture ($_{mix}^0$), and weathered mixture ($_{mix}$). A multiplier, often related to the efficiency of DIC-increase relative to alkalinity increase [20, 26, 27] is used to compute net CDR from f_d , hence an accurate estimate (\hat{f}_d) is the focus here. In this approach, $[M]_{mix}^0$ is calculated by measuring an immobile tracer (T) and using the following element-element mixing equation with baseline and feedstock ($_{fs}$) endmembers,

$$[M]_{mix}^0 = [M]_{bsln} + \frac{([T]_{mix} - [T]_{bsln})([M]_{fs} - [M]_{bsln})}{[T]_{fs} - [T]_{bsln}} \quad (2)$$

Here, heterogeneity can violate the basic assumptions of the mixing model if samples are not representative of the same geochemical “system” (Fig. 1). Uncertainty in these assumptions was initially considered in the context of analytical variance [19]. Building on this, Suhrhoff et al. (2024) evaluated how overall measurement variance, soil and feedstock compositions, and application rate influence the detectability of T upon amendment, as well as how the magnitude of f_d affects the ability to detect changes in M . They concluded that

measurement variance in T and the contrast between soil and feedstock compositions determine whether EW signals can be detected. However, given the inherent spatial heterogeneity in soils, it remains unclear whether scalable sampling plans can yield the low measurement variances required. Moreover, the detection of changes in elemental abundances does not guarantee accurate mixing calculations: even small measurement variances can yield apparent mixtures that fall outside of the theoretical mixing space [28].

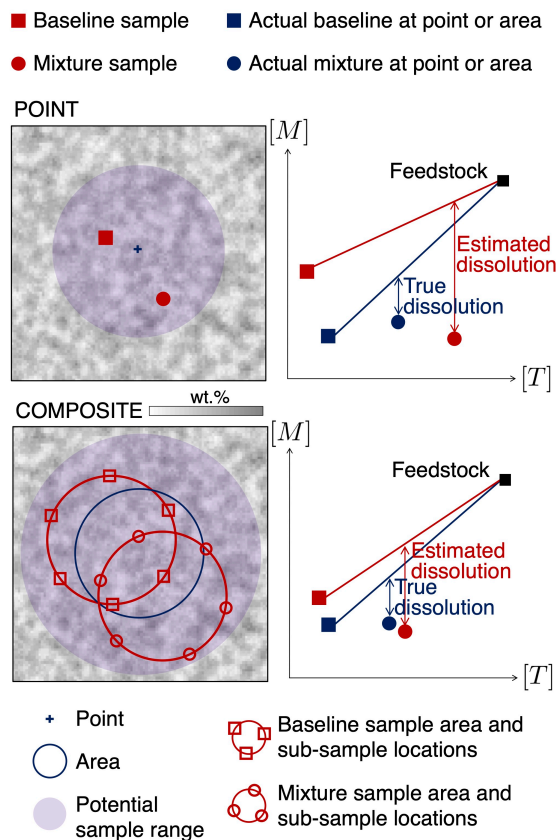


Figure 1: Illustration of how spatial uncertainty introduces error into feedstock dissolution calculations. The underlying mixing model assumes that baseline and mixture samples represent the same system or control volume. Given spatial heterogeneous soil compositions, this assumption may be interrupted by positioning error, tillage, and erosion, as well as sampling and preparation techniques and analytical precision. Composite sampling is commonly employed to mitigate spatial uncertainty by reducing sample variance.

These concerns highlight the need for a systematic approach to account for spatial heterogeneity in the design of EW verification protocols. To address this, we present a framework for incorporating spatial uncertainty into solid-phase measurements, starting with definition

of overall uncertainty requirements (*e.g.*, a maximum error and minimum confidence in \hat{f}_d), followed by variance propagation and sensitivity analysis (SA) to help define corresponding measurement variance requirements (*e.g.*, a maximum measurement variance and minimum confidence). We then use stochastic sampling simulations to infer a sampling approach that minimally meets these requirements and conclude with estimate and uncertainty reporting. This is detailed through the following steps:

1. Defining the uncertainty requirements and measurement model, the latter including explicit relationships between input and output uncertainty using hierarchical Bayesian principles.
2. Determining the maximum measurement variances that fulfill the overall uncertainty requirements using variance propagation and SA.
3. Defining the measurement variance requirements and sampling model, the latter involving stochastic simulation of spatial fields and composite sampling plans.
4. Designing a sampling plan that minimally meets the measurement variance requirements using the sampling model and SA; if infeasible, reconsider the overall uncertainty requirements or measurement model.
5. Reporting the final estimate and overall uncertainty, with traceable and reproducible uncertainty quantification.

Integrated Methods and Results

For EW, agricultural fields are typically chosen based on accessibility rather than a detailed understanding of soil properties and heterogeneity. The goal for the project developer is to perform minimal sampling while still accurately calculating the amount of dissolved feedstock and resultant CDR.

In this example, we illustrate how early characterization can be integral to EW site selection and monitoring design to increase the likelihood of precisely quantifying CDR. We assume deployment of a basaltic feedstock, though the approach is generalizable to any amendment. For mixing-based solid-phase verification of EW, the *measurement model* consists of equations (1) and (2), which are solved for f_d based on the measured baseline and, either the initial soil-feedstock mixture to determine application rates, or the mixture after some weathering has occurred [19]. Field trials [27, 29–38] report feedstock application rates ranging from 5 to 100 tons per hectare (ha), resulting in relatively low mass enrichment of 0.1–3% after mixing within the upper 20 cm of soil (Supp. 2). Another important consideration is the chemical differentiation between the feedstock and the baseline, which we analyze using the feedstock-baseline ratio of mean cation concentration ($\mu_M^{fs:bsln}$) and mean tracer concentration ($\mu_T^{fs:bsln}$).

The *sampling model* outlines the planned configuration for sampling, whether through discrete point samples or carefully homogenized composite samples, which we stochastically analyze to infer the measurement variance associated with different sampling strategies. Because the measurement model depends on the baseline, the sampling plan is typically fixed after the feedstock is applied, underscoring the need for a robust baseline sampling strategy. The uncertainty requirements are defined by operational constraints, such as the need to present a compensatory claim, and reflect the probability that the resulting estimate will fall within a specified range of the true value.

1. Uncertainty requirements and measurement model

The goal of this first step is to define the problem mathematically to allow for rigorous variance propagation and SA. In EW, the baseline variance in soil elemental abundances is typically unknown prior to site selection, and recent work [10] suggests that variability in an immobile tracer element tends to exceed that of base cations, thereby dominating the total uncertainty. Consequently, the site-specific variance in these elements determines whether a

given measurement approach is likely to fulfill the uncertainty requirements.

Uncertainty requirements

The uncertainty requirements are often defined by a standards development organization and, here, encapsulate:

- ϵ_{max} , the maximum relative error in \hat{f}_d and thus CDR.
- p_{min} , the minimum probability that the relative error in \hat{f}_d is less than ϵ_{max} .

For instance, a quantification standard might require 90% confidence ($p_{min} = 0.9$) that the reported CDR is within 10% of the true value ($\epsilon_{max} = 0.1$) [*e.g.*, 39]. There is no *a priori* guarantee, however, that any particular field deployment can meet these requirements for a specific site, due to the inherent variability in measurement conditions and system parameters.

We use ϕ to represent the outcome where the uncertainty requirements are fulfilled. Formally:

$$p(\epsilon \leq \epsilon_{max}) \geq p_{min} \implies \phi, \quad p(\epsilon \leq \epsilon_{max}) < p_{min} \implies \bar{\phi}, \quad (3)$$

where $\bar{\phi}$ indicates the requirements are not fulfilled.

Measurement model and parameter set

To calculate $p(\epsilon \leq \epsilon_{max})$ for different measurement approaches, we define a measurement model parameterized by θ . This model includes:

- a measurement function (*e.g.*, feedstock dissolution calculation, Eq. 1-2)
- input parameters (*e.g.*, M and T concentrations in the baseline, feedstock, and mixture)
- the function response (*e.g.*, fraction of feedstock dissolved, f_d),
- measurement variance of each input parameter (*e.g.*, spread of possible M and T measurement values given the point or composite sampling scheme), and

- operational parameters (*e.g.*, feedstock-baseline differentiation, application rate, true fraction dissolved).

For this measurement function (Eq. 1-2), the input parameters are $[M]_{bsln}$, $[M]_{fs}$, $[M]_{mix}$, $[T]_{bsln}$, $[T]_{fs}$, and $[T]_{mix}$. Due to spatial heterogeneity, baseline and mixture measurements may be highly variable, interrupting their assumed comparability (Fig. 2). To account for the impact of spatial heterogeneity, we consider each input parameter to have a distribution of possible measurement values, characterized by a mean (μ) and relative variance (v), which we will propagate through the measurement function in step 2. While measurement variance represents aggregate spatial and analytical uncertainty, we only consider spatial uncertainty in this study, as analytical uncertainty can be made negligible if necessary [19]. Accordingly, we define μ and v for the measurement distributions as follows:

Measurement means: We set μ_M^{bsln} and μ_T^{bsln} (baseline means) as constants at the simulation scale. We then specify feedstock-to-baseline ratios ($\mu_M^{fs:bsln}$, $\mu_T^{fs:bsln}$) to obtain mean feedstock concentrations. A uniform application rate (r_{app}) and uniform fraction dissolved (f_d) together determine the mean mixture concentrations after amendment and weathering. This f_d also serves as the “true” fraction against which estimation errors are calculated.

Measurement variances: We specify v_M and v_T , the (relative) measurement variances for baseline M and T . Due to feedstock mass enrichments of $< 3\%$, we assume the measurement variances of the soil-feedstock mixture are equal to the baseline v_M and v_T . The feedstock itself is assumed homogeneous (negligible variance).

Collectively, these parameters form the set θ . Since we want to test the impact of different measurement distributions and operational parameters on fulfilling the uncertainty requirements, we initially consider a wide range of possible values for each parameter. These ranges are used as bounds for uniform cumulative density functions (CDFs), denoted \hat{F} , and $\hat{F}(\theta)$ is the multivariate CDF describing the entire parameter space (Table 1). The next step

169 involves random sampling of this parameter space to rigorously evaluate the individual and
 170 joint impacts of each parameter on ϕ .

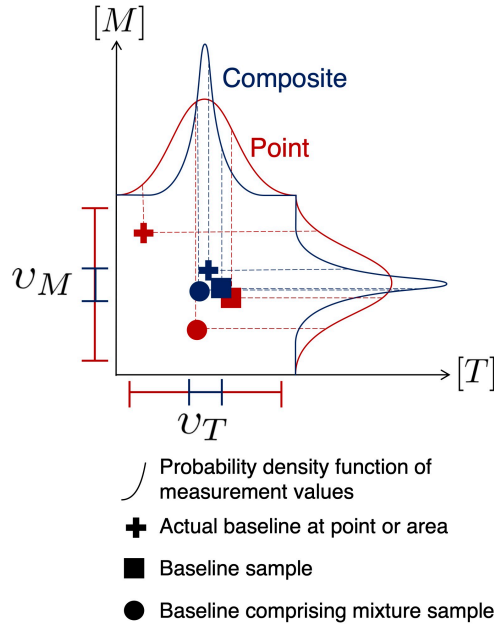


Figure 2: Illustration of how measurement variance (v) in cation (M) or tracer (T) concentrations may interrupt the assumed comparability of baseline and mixture samples to differing degrees depending on sampling approach. The goal of step 2 is to calculate how small v_M and v_T must be, or how narrow each probability density function of measurement values must be.

Table 1: Exploratory $\hat{F}(\theta)$, uniform distributions used for variance propagation and SA to determine measurement variance requirements.

| Parameter | Symbol | Units | Range (Transformation) | Source |
|--|-------------------|---------|---------------------------------------|---|
| Mean baseline concentrations | μ_M^{bsln} | mg/kg | $[7, 11]$ $(\ln[1100, 60000])$ | Lower and upper bound are lowest p_{10} and highest p_{90} of, for M , Ca , Mg , Na , and K and, for T , Ti , Cr , and Ni concentrations in upper 5 cm of CONUS soils [40]. |
| | μ_T^{bsln} | mg/kg | $[1, 9]$ $(\ln[2.72, 8100])$ | |
| Measurement variances | ψ_M | - | $[-9, -3]$ $(\ln[0.00012, 0.050])$ | Ranges chosen such that resulting variance propagation includes significant amounts of realizations that do and do not fulfill the uncertainty requirements. |
| | ψ_T | - | $[-9, -3]$ $(\ln[0.00012, 0.050])$ | |
| Feedstock-baseline mean concentration ratios | $\mu_M^{fs:bsln}$ | - | $[1, 75]$ | Ranges computed by dividing concentrations of selected elements in six basalt compositions reported by Lewis et al. [41] by corresponding p_{10} and p_{90} CONUS soil concentrations [40]. |
| | $\mu_T^{fs:bsln}$ | - | $[1, 49]$ | |
| Application rate | r_{app} | tons/ha | $[2, 100]$ | Annual rate of 5-100 t/ha across eleven EW field trials [27, 29-38]; lower bound extended to 2 t/ha based on conversations with EW PDs. |
| True fraction of feedstock dissolved | f_d | - | $[0.1, 0.3]$ | Range chosen based on values reported by Beerling et al. [30], where $\hat{f}_d = 0.12$ using Mg , 0.32 using Ca , four years after initial amendment. |

2. Determining maximum measurement variances

With the measurement model and parameter ranges established, next we analyze the sensitivity of the model and determine how small the measurement variances in M and T must be to meet the overall uncertainty requirements. This process involves propagating measurement variances through the measurement model (step 2.1), quantifying the influence of measurement variance on the accuracy of \hat{f}_d (step 2.2), and constraining operational parameters to set maximum measurement variances (v_{max}) for a specific deployment (step 2.3).

2.1 Propagating measurement variances through the measurement model

Here, we use nested Monte Carlo simulations to jointly vary the input means, measurement variances, and operational parameters encompassed by θ and, for each variation, compute the resulting $p(\epsilon \leq \epsilon_{max})$. This process begins with generating 10^4 *parameter realizations*, or samples of $\hat{F}(\theta)$. $\hat{F}(\theta)$ is a uniform multivariate distribution, meaning each parameter range in Table 1 is sampled from uniformly, and each realization represents a possible combination of baseline means (μ_M^{bsln} , μ_T^{bsln}), measurement variances (v_M , v_T), and operational parameters ($\mu_M^{fs:bsln}$, $\mu_T^{fs:bsln}$, r_{app} , f_d). $\hat{F}(\theta)$. For a given parameter realization, we use these values to construct Gaussian measurement distributions for $[M]_{bsln}$, $[M]_{mix}$, $[T]_{bsln}$, and $[T]_{mix}$, and we sample from these distributions to generate 10^4 *measurement realizations*. For each measurement realization, we compute \hat{f}_d and its relative error (ϵ), such that $p(\epsilon \leq \epsilon_{max})$ for each parameter realization is the fraction of its measurement realizations where $\epsilon \leq \epsilon_{max}$.

Results of these simulations indicate that ϕ is highly dependent on keeping the measurement variances below critical thresholds (Fig. 3), while other parameters, such as μ_M^{bsln} and μ_T^{bsln} , have minimal impact. Specifically, the distribution of $p(\epsilon \leq \epsilon_{max})$ shows a clear divide (Fig. 3A), indicating that while many realizations achieve ϕ , a significant number fail. The p_{10} - p_{90} grey-shaded regions in Fig. 3B illustrate the spread of simulation outcomes across each parameter range—shaded regions that extend above p_{min} (red-dashed line) indicate parameter values for the realizations that achieved ϕ in Fig. 3A. Conversely, the unshaded

regions above p_{min} indicate that high v_M and v_T and low r_{app} values will likely not result in ϕ .

The correlations among the expected $p(\epsilon \leq \epsilon_{max})$ —black p_{50} lines in Fig. 3B—and the individual parameters provide additional insight into sensitivities. Specifically, the conditional distributions of $p(\epsilon \leq \epsilon_{max})$ show a strong negative correlation with v_M and v_T , meaning high measurement variances make it unlikely to achieve $\leq 10\%$ error in \hat{f}_d (Fig. 3B). Intuitively, $\mu_M^{fs:bsln}$, $\mu_T^{fs:bsln}$, r_{app} , and true f_d show moderate positive correlations with $p(\epsilon \leq \epsilon_{max})$, indicating that greater values tend to increase the expected accuracy in \hat{f}_d . Overall, the wide range of outcomes here emphasizes the importance of considering all possible outcomes early in site selection and monitoring design.

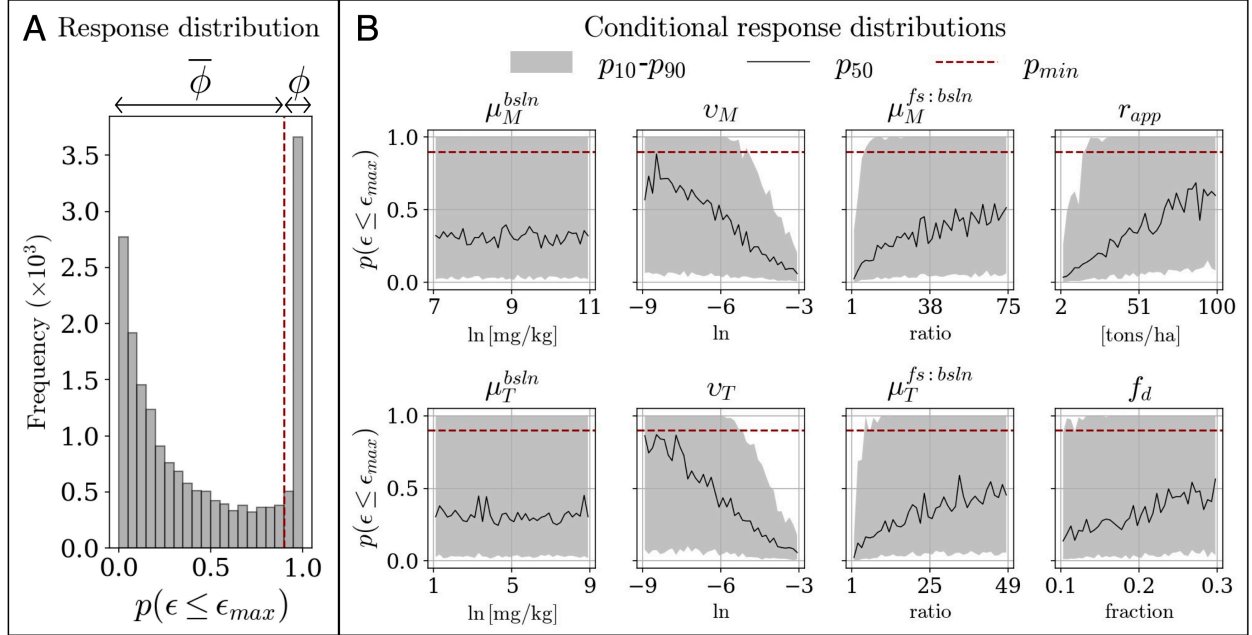


Figure 3: Exploratory SA of the influence of means (μ), measurement variances (v), and operational parameters on $p(\epsilon \leq 0.1)$, the probability that the relative error in \hat{f}_d is no greater than 10%, using the parameter ranges in Table 1. (A) shows the response across all 10⁴ realizations, with a red-dashed line separating the realizations that do (ϕ) and do not ($\bar{\phi}$) fulfill uncertainty requirements of $p(\epsilon \leq 0.1) \geq 90\%$ (p_{min}). (B) provides the conditional response distribution for each parameter.

2.2. Quantifying parameter influence on fulfilling the uncertainty requirements

To rigorously compare the sensitivity of ϕ to different parameters, we separate the 10^4 realizations of θ into one group that does fulfill the uncertainty requirements and one group that does not. This can be represented by partitioning $\hat{F}(\theta)$ into two conditional distributions, $\hat{F}(\theta|\phi)$ and $\hat{F}(\theta|\bar{\phi})$, and we can analyze the differences between these distributions to determine which parameters most significantly influence the outcome. A common way to quantify such sensitivities [42–45] is to compute the "distance" between $\hat{F}(\theta|\phi)$ and $\hat{F}(\theta|\bar{\phi})$ for each parameter (Fig. 4A), normalizing the parameter ranges to $[-1, 1]$ so they do not influence comparison of the distances. The resulting sensitivity rankings (Fig. 4B) highlight that ϕ is most influenced by v_M and v_T , and less so by r_{app} , $\mu_T^{fs:bsln}$, $\mu_M^{fs:bsln}$, and true f_d . Collectively, this emphasizes the dominant role of measurement variances in determining success.

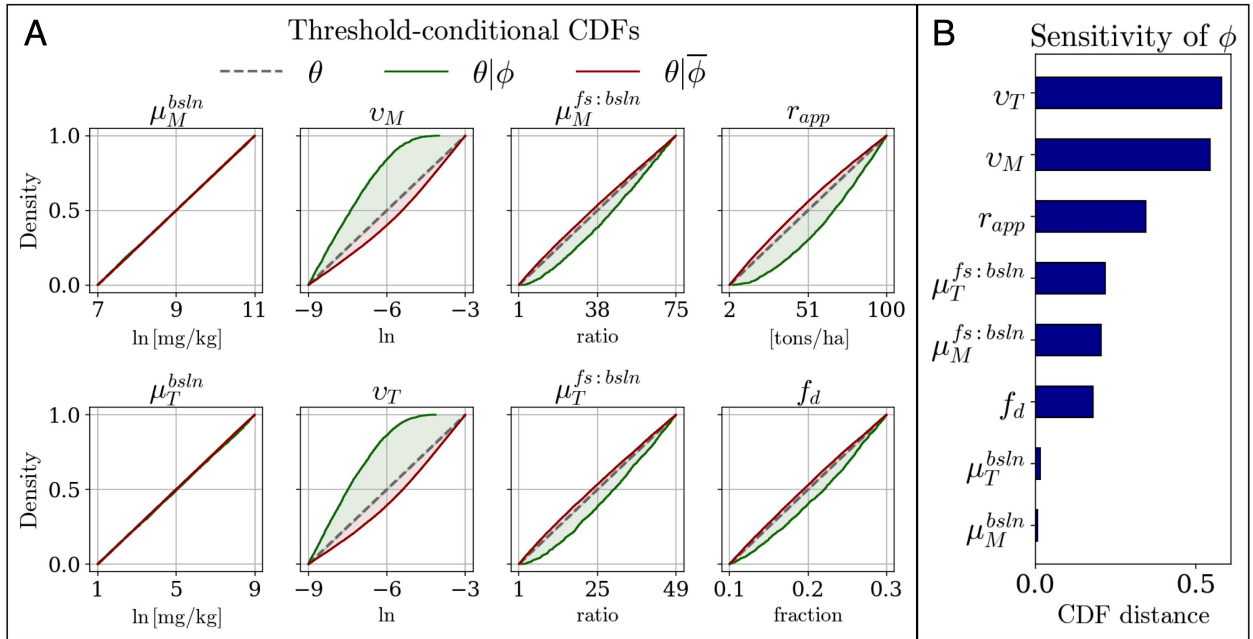


Figure 4: Distance-based sensitivity calculations for the exploratory SA in Fig. 3. (A) shows threshold-conditional CDFs (*e.g.*, partitions of the entire set of realizations (grey-dashed line) into realizations that did (green line) and did not (red line) fulfill uncertainty requirements, with shaded areas to visualize distances between CDFs. (B) provides a ranking of the parameters according to their influence on ϕ using this distance-based sensitivity metric.

2.3. Applying deployment-specific constraints and identify measurement variance limits

In practice, PDs can constrain certain parameters in θ , such as feedstock-baseline differentiation and application rate. For our theoretical deployment, we constrain $\mu_M^{fs:bsln}$ to 38 and $\mu_T^{fs:bsln}$ to 25 (midpoints from Table 1) and r_{app} to 40 tons/ha (median from Table 1). Performing the SA with these constraints (Fig. 5) reveals that the expected, or median, $p(\epsilon \leq \epsilon_{max})$ exceeds p_{min} for $\ln(v_M)$ and $\ln(v_T)$ less than approximately -7 (Fig. 5B). In contrast, the conditional response distributions for other parameters do not show an expected $p(\epsilon \leq \epsilon_{max})$ greater than p_{min} , as each distribution assumes values for all other parameters are randomly chosen from their respective ranges, thus incorporating effects from the entire ranges of v_M and v_T . While measurement variances are the primary control here, the true f_d will likely become significant after constraining v_M and v_T (Fig. 5C). This suggests that delaying intensive sampling, though also delaying return on investment to the PD, could be a key feature of profitable operations.

To determine specific measurement variance limits, we need to account for potential interactions between v_M and v_T by analyzing their joint conditional distribution (Fig. 6). It is also important to consider the entire $\hat{F}(\theta)$ when determining such limits. Using an exploratory $\hat{F}(\theta)$, this analysis shows almost no combinations of v_M and v_T that achieve ϕ (Fig. 6A). Using the constrained $\hat{F}(\theta)$, however, indicates the expected outcome is ϕ when both $\ln(v_M)$ and $\ln(v_T)$ are greater than approximately -6.5 (Fig. 6B). Since, for this example, v_M and v_T exert similar influences on ϕ , we select a single v_{max} of $e^{-6.5}$. The remaining analysis provides insight on combinations of inherent site characteristics and sampling designs that could likely adhere to this maximum using stochastic simulations of spatial variability and composite sampling.

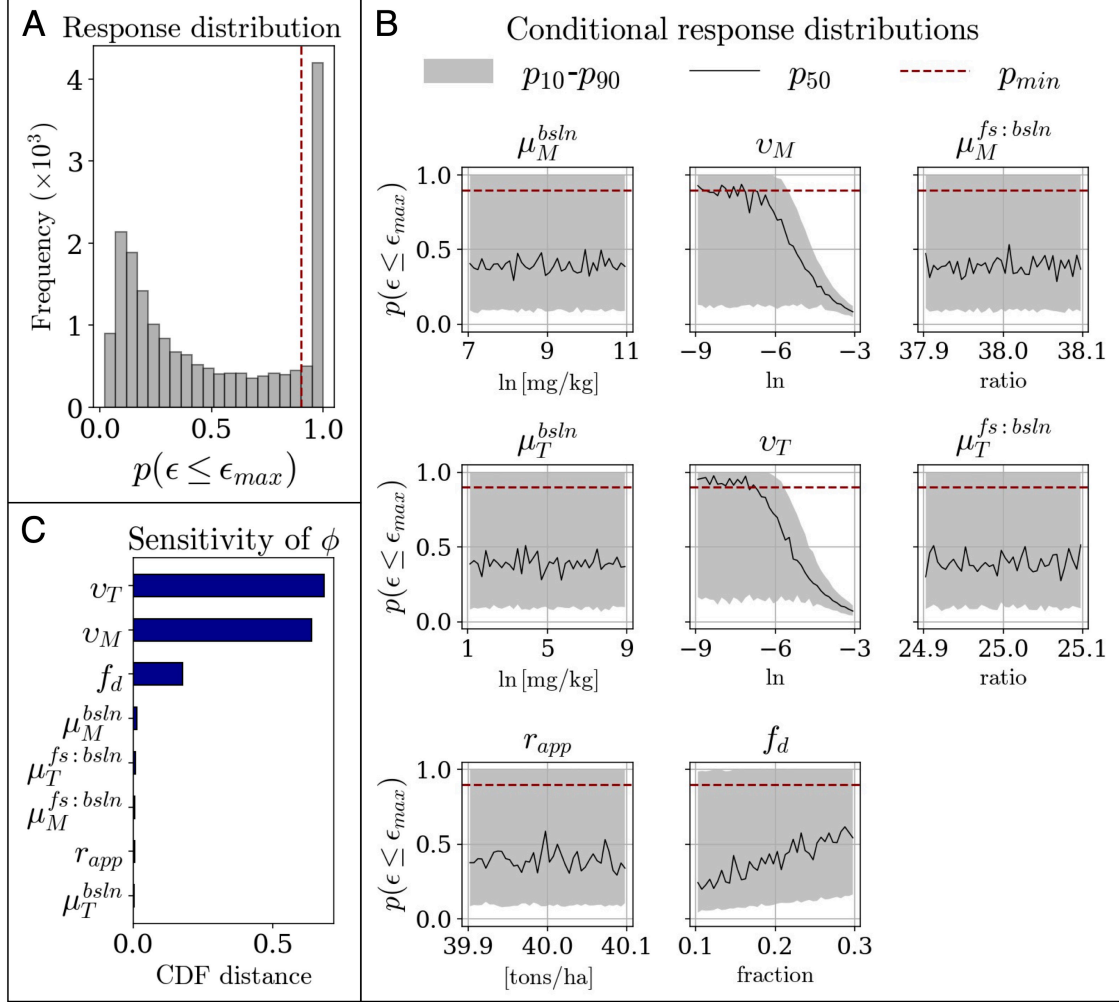


Figure 5: Deployment-specific SA where, relative to the exploratory SA in Fig. 3 and Fig. 4 and parameter ranges in Table 1, we apply constraints to soil-feedstock differentiation ($\mu_M^{fs:bsln} = 38$, $\mu_T^{fs:bsln} = 25$) and application rate ($r_{app} = 40$ tons/ha). (A) shows the updated response across all 10^4 realizations, (B) the updated conditional response distributions, and (C) the updated ranking of the parameters according to their influence on ϕ .

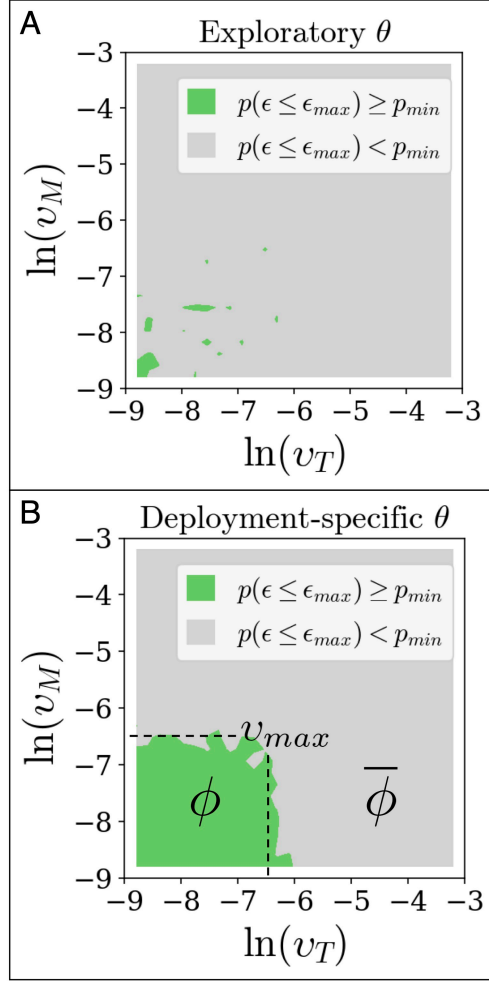


Figure 6: Combinations of base cation measurement variance (v_M) and immobile tracer measurement variance (v_T) that result in fulfilling uncertainty requirements (ϕ) of at least 90% likelihood of $\leq 10\%$ error in \hat{f}_d for (A) loosely constrained, exploratory parameter ranges and (B) constrained parameter ranges for a theoretical deployment where $\mu_M^{fs:bsln} = 38$, $\mu_T^{fs:bsln} = 25$, and $r_{app} = 40$ tons/ha.

3. Measurement variance requirements and sampling model

With v_{max} , we can simulate composite sampling to design a suitable sampling plan prior to execution. To determine sufficient sampling plans, one would in theory need to know the concentrations everywhere across the field site at high spatial resolution. Presumably, this would reveal lenses and patches of similar material, as opposed to a completely random distribution. Alternatively, we can create synthetic deployment fields based on models of spatial variability, an approach similar to that used in contaminant remediation [46–49] and measurement of soil organic carbon stocks [24, 50, 51], and sample them to develop measurement schemes that are robust across different types of spatial variability. In steps 3 and 4, the objective is to simulate spatial fields and composite sampling plans to determine approaches for achieving a measurement variance lower than v_{max} , and then refine these approaches to roughly minimize the number of samples.

Given that high-density sampling over large deployment areas is not feasible, we assume identification of a representative 1-ha plot for high-density sampling with low-density sampling still performed across the remainder of the area, similar to plot designs recommended in quantification standards [*e.g.*, 21]. Specifically, we are simulating 1 ha (10,000 m²) at 0.1-m resolution, thus using a 1,000 by 1,000 structured grid, which could analogously be described as 100 ha at 1-m resolution or 10,000 ha at 10-m. Ideally the resolution or "support size" mimics physical sample collection, *e.g.*, individual core area when simulating at the sub-sampling scale, or compositing area if each sample is representative of a grid cell.

Measurement variance requirements

Since we have chosen the same v_{max} of $e^{-6.5}$ for v_M and v_T , we can generally denote both $[M]$ and $[T]$ as an arbitrary spatial variable Z . Here, the measurement variance requirements for Z are defined by:

- v_{max} , the maximum allowable measurement variance in Z ,

- p_{min} , the minimum probability that the measurement variance in Z is below v_{max} .

For a given spatial field and sampling plan, $p(v \leq v_{max})$ is the likelihood that the resulting measurement variance (v) will be less than the maximum measurement variance (v_{max}). The measurement variance requirements are fulfilled when $p(v \leq v_{max})$ exceeds the probability threshold p_{min} , and the corresponding outcome is denoted ϕ_Z . Formally:

$$p(v \leq v_{max}) \geq p_{min} \implies \phi_Z, \quad p(v \leq v_{max}) < p_{min} \implies \bar{\phi}_Z. \quad (4)$$

Sampling model and parameter set

To compute $p(v \leq v_{max})$ for different combinations of spatial field and sampling plan, we first define a sampling model with parameter set θ_Z that encompasses stochastic simulation of heterogeneous spatial fields and composite sampling plans.

A spatial field's heterogeneity can be characterized by its spatial covariance, or strength of correlation between values at different locations depending on the physical distances separating them, often analytically represented by a covariance or semivariogram function [52]. These functions involve distribution parameters, here μ and CV expressed as natural logarithms, and a correlation length, λ , which describes how distant two locations can be and still have correlated values, or the "size" of the heterogeneities (Fig. 7A). Different analytical forms (*e.g.*, exponential, circular, Gaussian) are distinguished by the "smoothness" of the heterogeneities (Fig. 7B).

The parameter set θ_Z encompasses these spatial field parameters, as well as parametrization of a composite sampling plan, including the number of composite samples (n) and sub-samples (n_{sub}), radius of each composite sample (r_{app}), and margin of error intrinsic to the positioning device (e_{pos}) (Table 2).

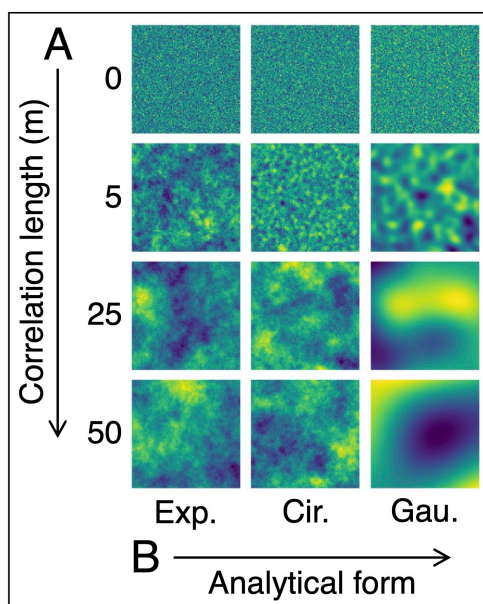


Figure 7: Examples of simulated 1-ha spatial fields with (A) increasing correlation lengths and (B) different analytical covariance models.

Table 2: Exploratory $\hat{F}(\theta_Z)$, uniform distributions used in stochastic spatial sampling simulations and SA to determine combinations of spatial field and sampling plan that result in measurement variances less than a target maximum.

| | Parameter | Symbol | Units | Transform | Range or Set |
|----------------------|---|-----------------|-------|-----------|--------------------------|
| Spatial field | True mean baseline concentration | μ_Z | mg/kg | ln | $\{1, 2, \dots, 11\}$ |
| | True baseline and mixture coefficient of variation | CV _Z | - | ln | $\{-8, -4, \dots, -1\}$ |
| | Distribution type | Dist. type | - | - | {normal, lognormal} |
| | Covariance model | Cov. model | - | - | {exponential, circular} |
| | Correlation length | λ_Z | m | - | $\{0, 10, 25, 50, 100\}$ |
| | Radius of each composite sample | r_c | m | - | $[0.5, 5]$ |
| Sampling plan | Number of randomly located composite samples | n | - | - | $\{1, 2, \dots, 30\}$ |
| | Number of sub-samples, collected at equal intervals along circumference of composite area | n_{sub} | - | - | $\{3, 4, \dots, 15\}$ |
| | Margin of error intrinsic to positioning device | e_{pos} | m | - | $[1, 10]$ |

4. Designing a sufficient sampling plan

With the measurement variance requirements and sampling model established, we can now stochastically analyze the model to determine a minimally sufficient sampling plan and evaluate its feasibility. This involves quantifying the relative influence of spatial heterogeneity and sampling parameters on fulfilling the variance requirements (step 4.1) then applying deployment-specific constraints to identify sufficient sampling plans and refining them to a specific plan (step 4.2).

4.1. Quantifying influence of spatial heterogeneity and sampling parameters on fulfilling measurement variance requirements

To partition the parameter space $\hat{F}(\theta_Z)$ into $\hat{F}(\theta_Z|\phi_Z)$ and $\hat{F}(\theta_Z|\bar{\phi}_Z)$ for sensitivity analysis, we use nested Monte Carlo simulations to compute $p(v \leq v_{max})$ for 10^4 realizations of θ_Z . After first generating the spatial field, we choose random locations for the n composite samples. For a single configuration of random locations, we simulate 100 rounds of composite sampling, computing the mean Z each time, and v as the relative variance of the 100 means. Considering a PD would only sample a handful of times throughout the course of a deployment, these 100 rounds represent the theoretical variability introduced by random positioning error and inconsistent orientation of sub-samples over a heterogeneous field. In the context of solid-phase EW verification, this formulation assumes the sampling plan is fixed with baseline sampling, and the f_d calculation uses the mean of all n samples rather than each sample individually. Altogether, for a single parameter realization of θ_Z , we simulate 100 different configurations of random locations, and $p(v \leq v_{max})$ is the portion of configurations where the inferred measurement variance is less than v_{max} .

Results of these nested simulations indicate that ϕ_Z is determined by the relative field-scale variance of Z (Fig. 8). Most realizations show an extremely low or extremely high likelihood of achieving a sufficiently small v (Fig. 8A), and there is a clear $\ln(\text{CV}_Z)$ threshold between -4 and -5 that dictates this behavior (Fig. 8B). The exact $\ln(\text{CV}_Z)$ threshold

is dependent on the maximum number of samples considered in the SA, though additional results show that increasing the maximum n from 30 to 100 still results in a threshold below -4. Overall, this highlights that spatial heterogeneity not only needs to be accurately constrained before designing a sampling plan, but may also determine whether any monitoring strategy can succeed.

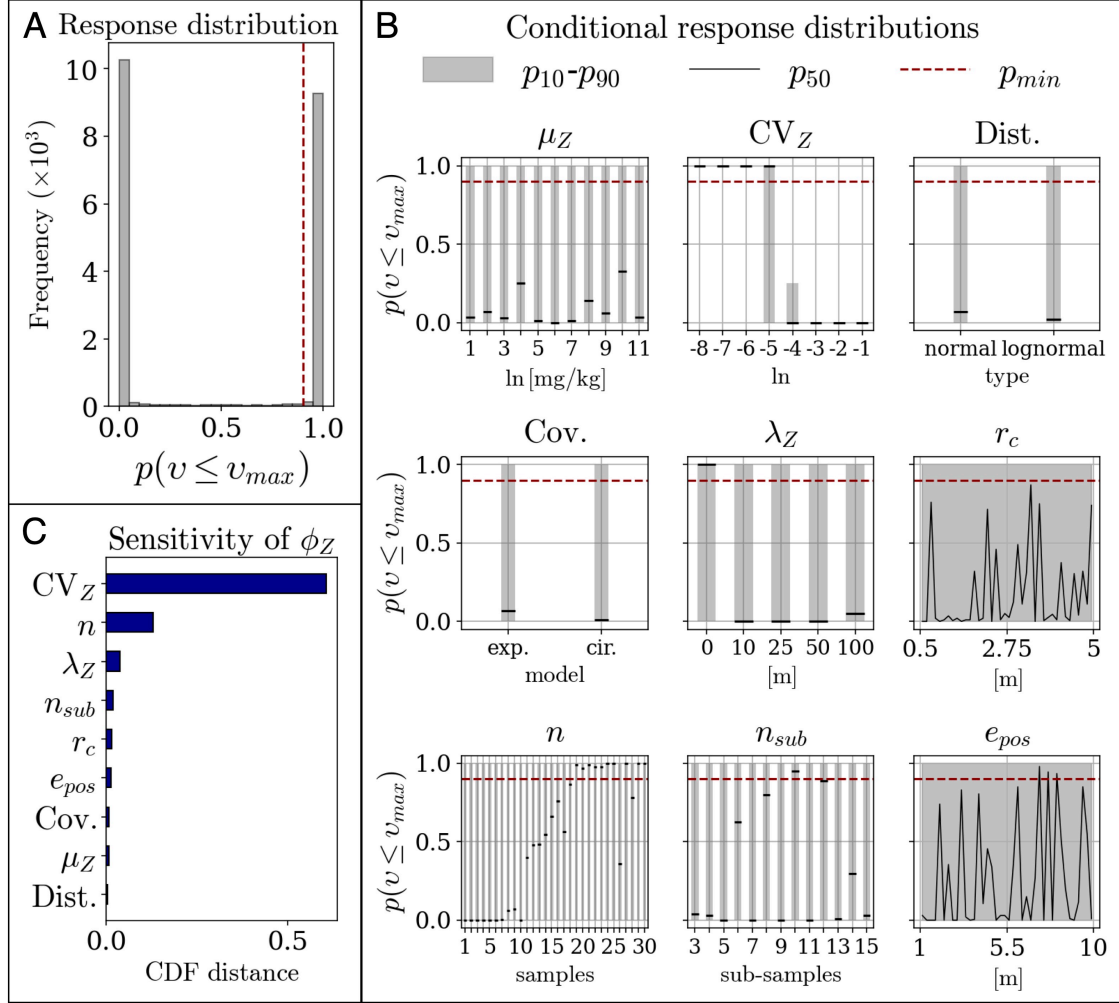


Figure 8: Exploratory SA of the influence of spatial heterogeneity and sampling plan on $p(v \leq e^{-6.5})$, the probability (p) that the inferred measurement variance (v) is less than a maximum measurement variance (v_{max}) of $e^{-6.5}$, using the parameter ranges in Table 2. (A) shows the response across all 10⁴ realizations, with a red-dashed line separating the realizations that do and do not fulfill requirements of at least 90% (p_{min}) likelihood of measurement variance less than $e^{-6.5}$. (B) provides the conditional response distribution for each parameter. (C) provides the ranking of the parameters according to their influence on ϕ_Z , using the distance-based metric illustrated in Fig. 4.

4.2 Applying deployment-specific constraints and refine to a specific sampling plan

To narrow down to a specific sampling plan, we first constrain relative field-scale variance, the major control on ϕ_Z . Though point sampling is typically necessary to capture the true CV, such data are sparse for soil elemental composition at ha-scales. Comparison to field studies [53–55] that have employed high-density point sampling of soil elemental concentrations (102–104 samples/ha) show ha-scale variances of $-3 \leq \ln(\text{CV}) \leq -1$ for base cations (Ca, Mg, Na, K) and select trace elements (Ti, Ni, Al, Fe) in temperate and semi-arid grassland, scrubland, forested, and agricultural settings (Fig. 9). These values, if generally representative, would not adhere to the threshold of -4 or -5 suggested by the analysis here (Fig. 9).

For a PD interested in constraining site-specific variance, further stochastic point-sampling simulations indicate that, given observed ranges [53–55], only up to about 20 point samples are needed to estimate CV to the nearest ln with 90% confidence (Fig. 10). In theory, these suggested sample sizes are directly applicable to larger scales, assuming correlation length is scaled with grid resolution, and the random spatial fields tested here encompass patterns observed at larger scales. Overall, this suggests it would be feasible to collect the preliminary measurements needed to infer operational scalability for a robust array of potential empirical constraints.

While lower than reported for soils to-date [53–55], we constrain $\ln(\text{CV}_Z)$ to -5 for our theoretical deployment and redo the SA (Fig. 11) to demonstrate next steps in monitoring design for feasibility assessment. Given this constraint, ϕ_Z becomes most sensitive to n , indicating at least 11 composite samples will result in $> 50\%$ likelihood, 18 samples $> 90\%$ likelihood, that v will be sufficiently small (Fig. 11B). It may be important to further constrain λ (Fig. 11C, Fig. 10), and alternative technologies, such as remote sensing [56], may be necessary to control costs.

Altogether, the analysis here indicates that spatial heterogeneity in soil concentrations should be the foremost consideration when designing sampling plans for solid-phase ver-

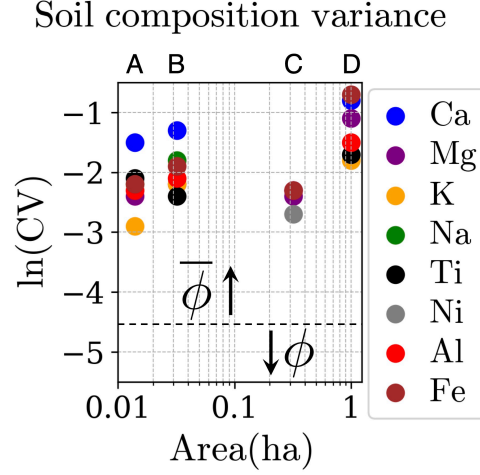


Figure 9: Relative variances of select soil elemental abundances in (A) scrubland in NW Spain ($n=203$, 0.014 ha, 0-10 cm depth) [55], (B) grassland in NW Spain ($n=186$, 0.032 ha, 0-10 cm depth) [55], (C) agricultural land in N Africa ($n=314$, 0.32 ha, 0-20 cm depth) [53], and (D) forested floodplain in NW Spain ($n=220$, 1 ha, 0-10 cm depth) [54], here shown relative to the approximate field-scale variance threshold partitioning fields between those that likely can (ϕ) and cannot ($\bar{\phi}$) fulfill the uncertainty requirements considered in this study.

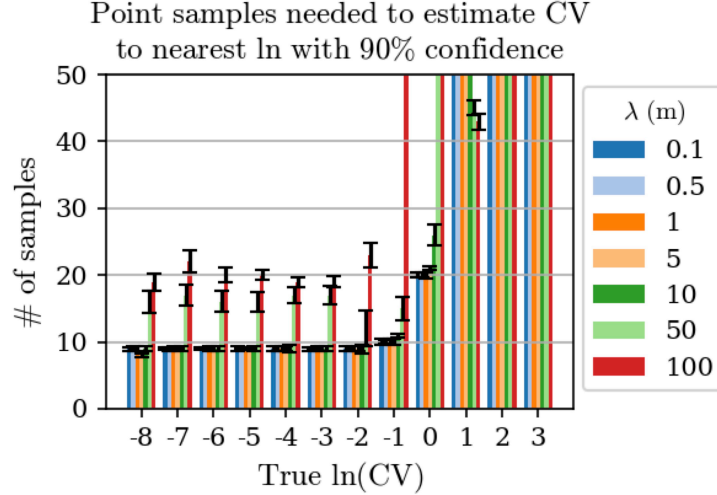


Figure 10: Simulation-based estimates of sample sizes needed to capture the coefficient of variation (CV) of a 1-ha (100 m x 100 m, 0.1-m resolution) lognormal spatial field to the nearest integer natural log (ln) with 90% confidence, considering different scales of spatial correlation (λ); errors bars represent the standard error across 10 spatial fields with different means.

ification of EW. Determining sufficient sampling plans requires preliminary constraints on relevant field-scale variances, and even minimally sufficient plans may be operationally infeasible, pointing toward reconsideration of the overall uncertainty requirements or measurement model.

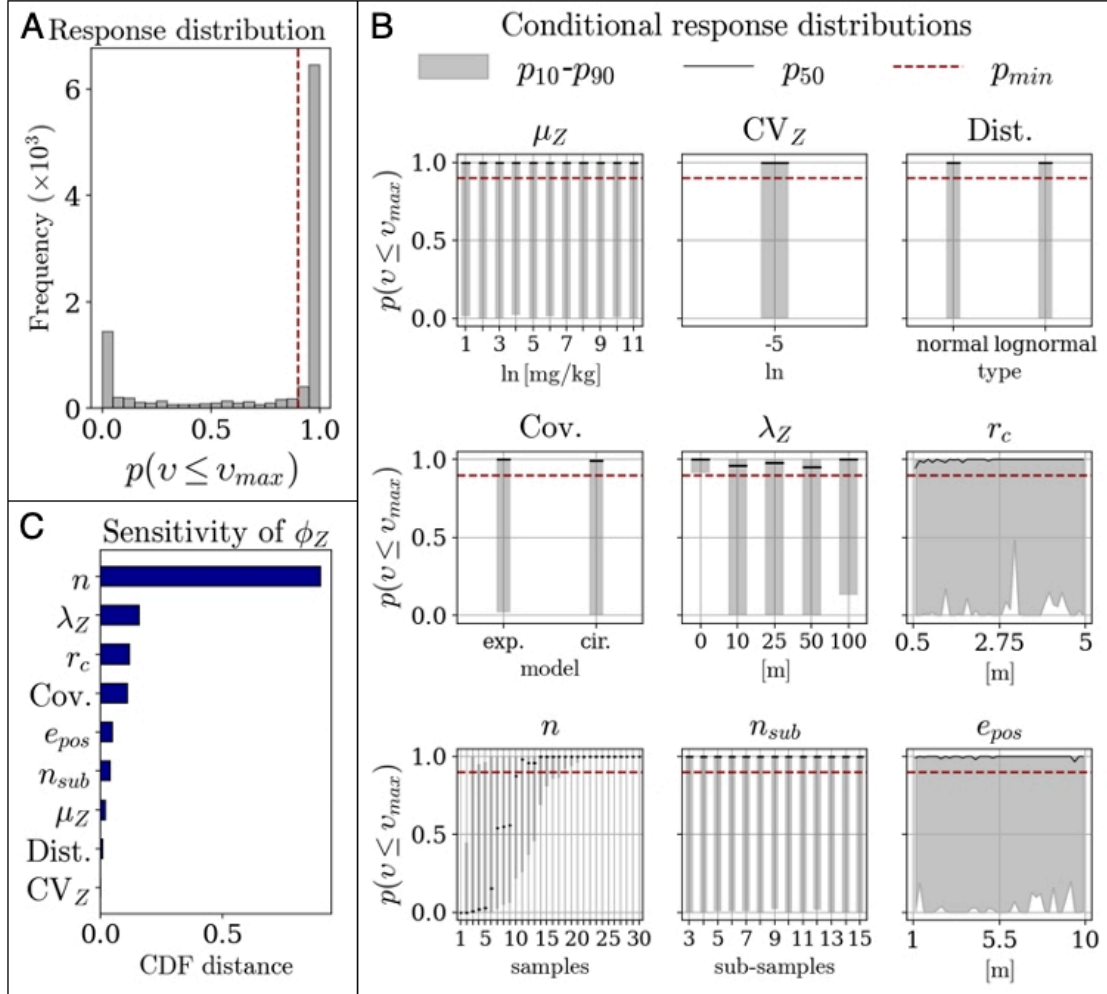


Figure 11: Deployment-specific SA where, relative to the exploratory SA in Fig. 8 and parameter ranges in Table 2, we constrain relative field-scale variance (CV_Z) to e^{-5} . (A) shows the updated response across all 10^4 parameter realizations, (B) the updated conditional response distributions, and (C) the updated ranking of parameters according to their influence on ϕ_Z .

5. Reporting the final estimate and uncertainty

In principle, reporting \hat{f}_d and its uncertainty is relatively straightforward following sample collection and analysis, as we have predetermined the margin of error and confidence in the calculation. However, transparency, reproducibility, and traceability are critical for both scientific and compensatory applications. In particular, procedural compliance should be separated from the inherent scientific and environmental uncertainty in evaluating whether a project achieved a result within quantifiable confidence bounds. Thus, in addition to providing the underlying measurement data and appropriate metadata, ideally including an ISGN framework [57], the reporting framework should systematically capture key uncertainty targets and measurement distributions as constrained with each sampling event. Supp. 3 provides an example reporting format, where all sources of uncertainty are documented, including deviations from initial estimated field variance, and the final estimate is presented with clearly defined error and confidence.

Discussion

The methodology we evaluate here emphasizes the importance of constructing a measurement model that is directly informed by uncertainty requirements. This is in contrast to the way EW field studies are traditionally designed, where the statistics are largely handled *ex post*. The probabilistic framework is sequential in nature and demonstrates how input variability propagates through a measurement model, unveiling the critical parameters influencing the overall uncertainty (steps 1-2). For EW, the measurement variances of base cation and tracer concentrations define the uncertainty in \hat{f}_d , indicating variance thresholds above which the uncertainty requirements will not be met. Stochastic spatial simulations (steps 3-4) inform composite sampling plans that adhere to the measurement variance thresholds, and constrained sensitivity analysis points to a minimally sufficient plan that can be evaluated for feasibility.

Importance of spatial heterogeneity

Our results demonstrate that in the absence of a thorough assessment of spatial variance, even well-composited samples may not adequately constrain measurement uncertainty, potentially resulting in intensive data collection that fails to achieve the confidence needed to assign CDR. To evaluate the scale of variability expected for agricultural and grassland soils, we reviewed studies [53–55] involving high-density (10^2 - 10^4 samples/ha) sampling. The relative variances in soil elemental abundances all exceed the maximum variance threshold identified in our analysis, suggesting that baseline soil heterogeneity may be too large for a mixing-model approach to produce reliable dissolution estimates (Fig. 9). While alternative solid-phase models, such as isotope mixing or bulk cation stocks, may be less sensitive to spatial heterogeneity, the analysis here poses an important consideration for EW, namely whether soil property distributions, and our ability to capture them with measurements, will fall within the requirements needed for verification frameworks.

Spatially coordinated field-scale solid-phase geochemical data is sparse in existing literature. Samples are usually collected in vertical configuration at single disperse sites, rather than laterally across the surface in a spatially explicit configuration, making it difficult to use the wealth of existing data to assess spatial variability. While the studies evaluated here show consistent variances over four land types within a geographical region, high-density soil data from other climates and geomorphic settings would be valuable in determining where field-scale geochemical variances are low enough for accurate solid-phase verification of EW. Spatial distributions of certain elements may also be correlated to textural parameters, such as clay content, or reflected in aboveground biomass. Rigorous confirmation and ground-truthing of potential proxies in early deployments could enable more efficient heterogeneity estimates in later deployments and thus more precise baseline sampling strategies at scale.

Here, we assume that spatial variance is the main contributor to measurement variance, though analytical uncertainty would be an additional factor for low-abundance chemical tracers. To account for this, future implementations can subtract analytical variance from the

maximum measurement variances identified in step 2, resulting in a lower target measurement variance in the sampling simulations. We also assume heterogeneity with depth can be implicitly captured in a 2-D representation of a sampling volume, which may not be true if stratigraphic variations with depth are widely inconsistent over a field.

A related challenge is the identification of intensively measured plots—simulated here at 1 ha, but can be larger— that are representative of project areas spanning tens-of-thousands of hectares. Quantifying the degree to which small-scale trials capture relevant spatial variability in larger landscapes remains a critical open question.

Implications

Collectively, simulating spatial variability and realistic sampling strategies can reduce logistical inefficiencies for EW and minimize the risk of failing to meet uncertainty requirements for CDR quantification. Effective verification of open-system CDR requires balancing standardized sampling guidelines with the flexibility to accommodate diverse field conditions, as well as managing tradeoffs between measurement costs and the certainty of outcomes. The proposed framework addresses these challenges by clearly defining uncertainty targets, allowing sampling plans to be rigorously evaluated prior to intensive field deployment. This transparent, multi-stage approach helps differentiate procedural compliance from the inherent scientific and environmental uncertainties affecting removal performance.

Acknowledgement

The authors gratefully acknowledge support from the Stanford Sustainability Accelerator (GHG-0012). BR acknowledges support from the Department of Energy Computational Science Graduate Fellowship (DE-SC0021110) and Stanford Data Science.

Supporting Information Available

- "Supp1_Derivations.pdf"
- "Supp2_Calculations.xlsx"
- "Supp3_ExampleReporting.xlsx"
- Simulation Data and Tools: <https://github.com/rogersdb/cz-spatial-uq>

References

- [1] Salvatore Calabrese et al. "Nano- to Global-Scale Uncertainties in Terrestrial Enhanced Weathering". In: *Environmental Science & Technology* 56.22 (Nov. 15, 2022), pp. 15261–15272. ISSN: 0013-936X, 1520-5851. DOI: 10.1021/acs.est.2c03163. URL: <https://pubs.acs.org/doi/10.1021/acs.est.2c03163> (visited on 04/07/2025).
- [2] Charlotte R. Levy et al. "Enhanced Rock Weathering for Carbon Removal–Monitoring and Mitigating Potential Environmental Impacts on Agricultural Land". In: *Environmental Science & Technology* 58.39 (Oct. 1, 2024), pp. 17215–17226. ISSN: 0013-936X, 1520-5851. DOI: 10.1021/acs.est.4c02368. URL: <https://pubs.acs.org/doi/10.1021/acs.est.4c02368> (visited on 04/01/2025).
- [3] Katie Lebling, Danielle Riedl, and Haley Leslie-Bole. "Measurement, Reporting, and Verification for Novel Carbon Dioxide Removal in US Federal Policy". In: *World Resources Institute* (June 2024). DOI: 10.46830/wriwp.23.00044. URL: https://www.wri.org/research/measurement-reporting-and-verification-novel-carbon-dioxide-removal?auHash=rLtKBvDkX0auKYcYp_RiaIDTlXpQAIy2kLH21DTMNZs (visited on 04/18/2025).
- [4] Leo Mercer and Josh Burke. "Strengthening MRV standards for greenhouse gas removals to improve climate change governance". In: (2023).

- [5] D.A.C. Manning et al. “Carbonate precipitation in artificial soils produced from basaltic quarry fines and composts: An opportunity for passive carbon sequestration”. In: *International Journal of Greenhouse Gas Control* 17 (Sept. 2013), pp. 309–317. ISSN: 17505836. DOI: 10.1016/j.ijggc.2013.05.012. URL: <https://linkinghub.elsevier.com/retrieve/pii/S1750583613002156> (visited on 02/19/2024).
- [6] Jens Hartmann et al. “Enhanced chemical weathering as a geoengineering strategy to reduce atmospheric carbon dioxide, supply nutrients, and mitigate ocean acidification: ENHANCED WEATHERING”. In: *Reviews of Geophysics* 51.2 (Apr. 2013), pp. 113–149. ISSN: 87551209. DOI: 10.1002/rog.20004. URL: <http://doi.wiley.com/10.1002/rog.20004> (visited on 02/11/2023).
- [7] IPCC. *Global Warming of 1.5°C: IPCC Special Report on Impacts of Global Warming of 1.5°C above Pre-industrial Levels in Context of Strengthening Response to Climate Change, Sustainable Development, and Efforts to Eradicate Poverty*. 1st ed. Cambridge University Press, 2018. ISBN: 978-1-00-915794-0 978-1-00-915795-7. DOI: 10.1017/9781009157940. URL: <https://www.cambridge.org/core/product/identifier/9781009157940/type/book> (visited on 05/27/2025).
- [8] NASEM. *Negative Emissions Technologies and Reliable Sequestration: A Research Agenda*. Pages: 25259. Washington, D.C.: National Academies Press, Mar. 8, 2019. ISBN: 978-0-309-48452-7. DOI: 10.17226/25259. URL: <https://www.nap.edu/catalog/25259> (visited on 05/27/2025).
- [9] David J. Beerling et al. “Potential for large-scale CO₂ removal via enhanced rock weathering with croplands”. In: *Nature* 583.7815 (July 9, 2020), pp. 242–248. ISSN: 0028-0836, 1476-4687. DOI: 10.1038/s41586-020-2448-9. URL: <http://www.nature.com/articles/s41586-020-2448-9> (visited on 02/06/2023).
- [10] Tim Jesper Suhrhoff et al. “A tool for assessing the sensitivity of soil-based approaches for quantifying enhanced weathering: a US case study”. In: *Frontiers in Climate* 6

- (Apr. 12, 2024), p. 1346117. ISSN: 2624-9553. DOI: 10.3389/fclim.2024.1346117. URL: <https://www.frontiersin.org/articles/10.3389/fclim.2024.1346117/full> (visited on 04/16/2024).
- [11] L. A. Derry, O. A. Chadwick, and S. Porder. “Estimation of Carbon Dioxide Removal via Enhanced Weathering”. In: *Global Change Biology* 31.2 (Feb. 2025), e70067. ISSN: 1354-1013, 1365-2486. DOI: 10.1111/gcb.70067. URL: <https://onlinelibrary.wiley.com/doi/10.1111/gcb.70067> (visited on 04/09/2025).
- [12] H Lin. “Earth’s Critical Zone and hydrogeology: concepts, characteristics, and advances”. In: *Hydrol. Earth Syst. Sci.* (2010).
- [13] H. Vereecken et al. “Modeling Soil Processes: Review, Key Challenges, and New Perspectives”. In: *Vadose Zone Journal* 15.5 (May 2016), pp. 1–57. ISSN: 1539-1663, 1539-1663. DOI: 10.2136/vzj2015.09.0131. URL: <https://access.onlinelibrary.wiley.com/doi/10.2136/vzj2015.09.0131> (visited on 04/23/2025).
- [14] Maya Almaraz et al. “Methods for determining the CO₂ removal capacity of enhanced weathering in agronomic settings”. In: *Frontiers in Climate* 4 (Dec. 16, 2022), p. 970429. ISSN: 2624-9553. DOI: 10.3389/fclim.2022.970429. URL: <https://www.frontiersin.org/articles/10.3389/fclim.2022.970429/full> (visited on 11/22/2023).
- [15] Matthew O. Clarkson et al. “A review of measurement for quantification of carbon dioxide removal by enhanced weathering in soil”. In: *Frontiers in Climate* 6 (June 19, 2024), p. 1345224. ISSN: 2624-9553. DOI: 10.3389/fclim.2024.1345224. URL: <https://www.frontiersin.org/articles/10.3389/fclim.2024.1345224/full> (visited on 09/22/2024).
- [16] William J. Knapp et al. “Quantifying CO₂ Removal at Enhanced Weathering Sites: a Multiproxy Approach”. In: *Environmental Science & Technology* 57.26 (July 4, 2023),

- pp. 9854–9864. ISSN: 0013-936X, 1520-5851. DOI: 10.1021/acs.est.3c03757. URL: <https://pubs.acs.org/doi/10.1021/acs.est.3c03757> (visited on 04/01/2025).
- [17] Heath Hasemer, Justin Borevitz, and Wolfram Buss. “Measuring enhanced weathering: inorganic carbon-based approaches may be required to complement cation-based approaches”. In: *Frontiers in Climate* 6 (Sept. 3, 2024), p. 1352825. ISSN: 2624-9553. DOI: 10.3389/fclim.2024.1352825. URL: <https://www.frontiersin.org/articles/10.3389/fclim.2024.1352825/full> (visited on 09/22/2024).
- [18] Lukas Rieder, Thorben Amann, and Jens Hartmann. “Soil electrical conductivity as a proxy for enhanced weathering in soils”. In: *Frontiers in Climate* 5 (Jan. 11, 2024), p. 1283107. ISSN: 2624-9553. DOI: 10.3389/fclim.2023.1283107. URL: <https://www.frontiersin.org/articles/10.3389/fclim.2023.1283107/full> (visited on 02/18/2024).
- [19] Tom Reershemius et al. “Initial Validation of a Soil-Based Mass-Balance Approach for Empirical Monitoring of Enhanced Rock Weathering Rates”. In: *Environmental Science & Technology* (Nov. 14, 2023), acs.est.3c03609. ISSN: 0013-936X, 1520-5851. DOI: 10.1021/acs.est.3c03609. URL: <https://pubs.acs.org/doi/10.1021/acs.est.3c03609> (visited on 11/30/2023).
- [20] P. Renforth. “The potential of enhanced weathering in the UK”. In: *International Journal of Greenhouse Gas Control* 10 (Sept. 2012), pp. 229–243. ISSN: 17505836. DOI: 10.1016/j.ijggc.2012.06.011. URL: <https://linkinghub.elsevier.com/retrieve/pii/S1750583612001466> (visited on 03/29/2024).
- [21] Kevin Sutherland et al. *Enhanced Weathering in Agriculture*. Version 1.1.0. Jan. 22, 2025. URL: <https://registry.isometric.com/protocol/enhanced-weathering-agriculture#determination-2>.
- [22] puro.earth. *Enhanced Rock Weathering Methodology for CO₂ Removal*. Version 2022 v. 2. 2024.

- [23] Ronald L. Wasserstein, Allen L. Schirm, and Nicole A. Lazar. “Moving to a World Beyond “ $p < 0.05$ ””. In: *The American Statistician* 73 (sup1 Mar. 29, 2019), pp. 1–19. ISSN: 0003-1305, 1537-2731. DOI: 10.1080/00031305.2019.1583913. URL: <https://www.tandfonline.com/doi/full/10.1080/00031305.2019.1583913> (visited on 04/22/2025).
- [24] M.A. Bradford et al. “Testing the feasibility of quantifying change in agricultural soil carbon stocks through empirical sampling”. In: *Geoderma* 440 (Dec. 2023), p. 116719. ISSN: 00167061. DOI: 10.1016/j.geoderma.2023.116719. URL: <https://linkinghub.elsevier.com/retrieve/pii/S0016706123003968> (visited on 04/08/2025).
- [25] George H Brimhall and William E Dietrich. “Constitutive mass balance relations between chemical composition, volume, density, porosity, and strain in metasomatic hydrochemical systems: Results on weathering and pedogenesis”. In: (1986).
- [26] Matteo B. Bertagni and Amilcare Porporato. “The Carbon-Capture Efficiency of Natural Water Alkalinization: Implications For Enhanced weathering”. In: *Science of The Total Environment* 838 (Sept. 2022), p. 156524. ISSN: 00489697. DOI: 10.1016/j.scitotenv.2022.156524. URL: <https://linkinghub.elsevier.com/retrieve/pii/S004896972203621X> (visited on 05/28/2025).
- [27] Christiana Dietzen and Minik T. Rosing. “Quantification of CO₂ uptake by enhanced weathering of silicate minerals applied to acidic soils”. In: *International Journal of Greenhouse Gas Control* 125 (May 2023), p. 103872. ISSN: 17505836. DOI: 10.1016/j.ijggc.2023.103872. URL: <https://linkinghub.elsevier.com/retrieve/pii/S1750583623000427> (visited on 10/20/2023).
- [28] Surendra P. Verma. “Error propagation in geochemical modeling of trace elements in two-component mixing”. In: *Geofísica Internacional* 37.4 (Oct. 1, 1998), pp. 327–338. ISSN: 0016-7169. DOI: 10.22201/igeof.00167169p.1998.37.4.517. URL: [http:](http://)

- `//revistagi.geofisica.unam.mx/index.php/RGI/article/view/622` (visited on 04/08/2025).
- [29] Ilsa B. Kantola et al. “Improved net carbon budgets in the US Midwest through direct measured impacts of enhanced weathering”. In: *Global Change Biology* 29.24 (Dec. 2023), pp. 7012–7028. ISSN: 1354-1013, 1365-2486. DOI: 10.1111/gcb.16903. URL: <https://onlinelibrary.wiley.com/doi/10.1111/gcb.16903> (visited on 05/04/2024).
- [30] David J. Beerling et al. “Enhanced weathering in the US Corn Belt delivers carbon removal with agronomic benefits”. In: *Proceedings of the National Academy of Sciences* 121.9 (Feb. 27, 2024), e2319436121. ISSN: 0027-8424, 1091-6490. DOI: 10.1073/pnas.2319436121. URL: <https://pnas.org/doi/10.1073/pnas.2319436121> (visited on 03/25/2024).
- [31] Fuxing Guo et al. “Crop productivity and soil inorganic carbon change mediated by enhanced rock weathering in farmland: A comparative field analysis of multi-agroclimatic regions in central China”. In: *Agricultural Systems* 210 (Aug. 2023), p. 103691. ISSN: 0308521X. DOI: 10.1016/j.agsy.2023.103691. URL: <https://linkinghub.elsevier.com/retrieve/pii/S0308521X23000963> (visited on 11/22/2023).
- [32] Christina S. Larkin et al. “Quantification of CO₂ removal in a large-scale enhanced weathering field trial on an oil palm plantation in Sabah, Malaysia”. In: *Frontiers in Climate* 4 (Aug. 30, 2022), p. 959229. ISSN: 2624-9553. DOI: 10.3389/fclim.2022.959229. URL: <https://www.frontiersin.org/articles/10.3389/fclim.2022.959229/full> (visited on 05/11/2023).
- [33] Fangna Wang et al. “Wollastonite powder application increases rice yield and CO₂ sequestration in a paddy field in Northeast China”. In: *Plant and Soil* (Feb. 28, 2024). ISSN: 0032-079X, 1573-5036. DOI: 10.1007/s11104-024-06570-5. URL: <https://link.springer.com/10.1007/s11104-024-06570-5> (visited on 07/06/2024).

- [34] Kirstine Skov et al. “Initial agronomic benefits of enhanced weathering using basalt: A study of spring oat in a temperate climate”. In: *PLOS ONE* 19.3 (Mar. 27, 2024). Ed. by Timothy Omara, e0295031. ISSN: 1932-6203. DOI: 10.1371/journal.pone.0295031. URL: <https://dx.plos.org/10.1371/journal.pone.0295031> (visited on 07/06/2024).
- [35] Iris O Holzer, Mallika A Nocco, and Benjamin Z Houlton. “Direct evidence for atmospheric carbon dioxide removal via enhanced weathering in cropland soil”. In: *Environmental Research Communications* 5.10 (Oct. 1, 2023), p. 101004. ISSN: 2515-7620. DOI: 10.1088/2515-7620/acfd89. URL: <https://iopscience.iop.org/article/10.1088/2515-7620/acfd89> (visited on 10/19/2023).
- [36] Frank McDermott et al. “Enhanced weathering for CO₂ removal using carbonate-rich crushed returned concrete; a pilot study from SE Ireland”. In: *Applied Geochemistry* 169 (Aug. 2024), p. 106056. ISSN: 08832927. DOI: 10.1016/j.apgeochem.2024.106056. URL: <https://linkinghub.elsevier.com/retrieve/pii/S0883292724001616> (visited on 07/06/2024).
- [37] Xavier Dupla et al. “Let the dust settle: Impact of enhanced rock weathering on soil biological, physical, and geochemical fertility”. In: *Science of The Total Environment* 954 (Dec. 2024), p. 176297. ISSN: 00489697. DOI: 10.1016/j.scitotenv.2024.176297. URL: <https://linkinghub.elsevier.com/retrieve/pii/S0048969724064532> (visited on 12/18/2024).
- [38] Noah W. Sokol et al. “Reduced accrual of mineral-associated organic matter after two years of enhanced rock weathering in cropland soils, though no net losses of soil organic carbon”. In: *Biogeochemistry* 167.8 (July 23, 2024), pp. 989–1005. ISSN: 1573-515X. DOI: 10.1007/s10533-024-01160-0. URL: <https://link.springer.com/10.1007/s10533-024-01160-0> (visited on 12/18/2024).

- [39] The Earth Partners LLC. *VCS Module VMD0021: Estimation of Stocks in the Soil Carbon Pool*. Version 1.0. Nov. 16, 2012. URL: <https://verra.org/methodologies/vm0021-soil-carbon-quantification-methodology-v1-0/>.
- [40] David Smith et al. *Geochemical and Mineralogical Maps, with Interpretation, for Soils of the Conterminous United States*. 2019. DOI: <https://doi.org/10.3133/sir20175118>.
- [41] Amy L. Lewis et al. “Effects of mineralogy, chemistry and physical properties of basalts on carbon capture potential and plant-nutrient element release via enhanced weathering”. In: *Applied Geochemistry* 132 (Sept. 2021), p. 105023. ISSN: 08832927. DOI: 10.1016/j.apgeochem.2021.105023. URL: <https://linkinghub.elsevier.com/retrieve/pii/S0883292721001554> (visited on 02/06/2023).
- [42] R Spear. “Eutrophication in peel inlet—II. Identification of critical uncertainties via generalized sensitivity analysis”. In: *Water Research* 14.1 (1980), pp. 43–49. ISSN: 00431354. DOI: 10.1016/0043-1354(80)90040-8. URL: <https://linkinghub.elsevier.com/retrieve/pii/0043135480900408> (visited on 11/27/2024).
- [43] A. Saltelli, ed. *Sensitivity analysis in practice: a guide to assessing scientific models*. Hoboken, NJ: Wiley, 2004. 219 pp. ISBN: 978-0-470-87093-8.
- [44] Céline Scheidt and Jef Caers. “Representing Spatial Uncertainty Using Distances and Kernels”. In: *Mathematical Geosciences* 41.4 (May 2009), pp. 397–419. ISSN: 1874-8961, 1874-8953. DOI: 10.1007/s11004-008-9186-0. URL: <http://link.springer.com/10.1007/s11004-008-9186-0> (visited on 11/17/2024).
- [45] Darryl Fenwick, Céline Scheidt, and Jef Caers. “Quantifying Asymmetric Parameter Interactions in Sensitivity Analysis: Application to Reservoir Modeling”. In: *Mathematical Geosciences* 46.4 (May 2014), pp. 493–511. ISSN: 1874-8961, 1874-8953. DOI: 10.1007/s11004-014-9530-5. URL: <http://link.springer.com/10.1007/s11004-014-9530-5> (visited on 11/24/2024).

- [46] George Christakos and Ricardo A. Olea. “Sampling design for spatially distributed hydrogeologic and environmental processes”. In: *Advances in Water Resources* 15.4 (Jan. 1992), pp. 219–237. ISSN: 03091708. DOI: 10.1016/0309-1708(92)90008-P. URL: <https://linkinghub.elsevier.com/retrieve/pii/030917089290008P> (visited on 02/04/2025).
- [47] Hwong-wen Ma and Chih-Chen Chang. “Assessment of the value of reducing uncertainty by sampling in a groundwater remediation system”. In: *Science of The Total Environment* 402.1 (Aug. 25, 2008), pp. 9–17. ISSN: 00489697. DOI: 10.1016/j.scitotenv.2008.04.034. URL: <https://linkinghub.elsevier.com/retrieve/pii/S004896970800452X> (visited on 02/04/2025).
- [48] Hélène Demougeot-Renard, Chantal De Fouquet, and Philippe Renard. “Forecasting the Number of Soil Samples Required to Reduce Remediation Cost Uncertainty”. In: *Journal of Environmental Quality* 33.5 (Sept. 2004), pp. 1694–1702. ISSN: 0047-2425, 1537-2537. DOI: 10.2134/jeq2004.1694. URL: <https://access.onlinelibrary.wiley.com/doi/10.2134/jeq2004.1694> (visited on 04/16/2025).
- [49] S. Verstraete and M. Van Meirvenne. “A multi-stage sampling strategy for the delineation of soil pollution in a contaminated brownfield”. In: *Environmental Pollution* 154.2 (July 2008), pp. 184–191. ISSN: 02697491. DOI: 10.1016/j.envpol.2007.10.014. URL: <https://linkinghub.elsevier.com/retrieve/pii/S0269749107005015> (visited on 04/16/2025).
- [50] R. M. Lark. “Estimating the regional mean status and change of soil properties: two distinct objectives for soil survey”. In: *European Journal of Soil Science* 60.5 (Oct. 2009), pp. 748–756. ISSN: 1351-0754, 1365-2389. DOI: 10.1111/j.1365-2389.2009.01156.x. URL: <https://bsssjournals.onlinelibrary.wiley.com/doi/10.1111/j.1365-2389.2009.01156.x> (visited on 04/16/2025).

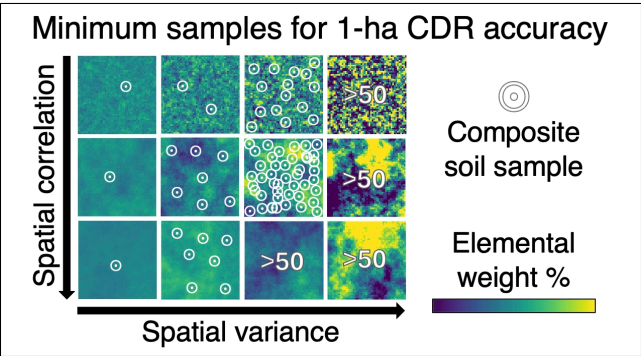
- [51] Eric Potash et al. “Measure-and-remeasure as an economically feasible approach to crediting soil organic carbon at scale”. In: *Environmental Research Letters* 20.2 (Feb. 1, 2025), p. 024025. ISSN: 1748-9326. DOI: 10.1088/1748-9326/ada16c. URL: <https://iopscience.iop.org/article/10.1088/1748-9326/ada16c> (visited on 04/16/2025).
- [52] Richard Webster and Margaret A. Oliver. *Geostatistics for environmental scientists*. 2nd ed. Statistics in practice. Chichester: John Wiley & sons, 2007. ISBN: 978-0-470-02858-2.
- [53] Akissa Bahri, Ronny Berndtsson, and Kenji Jinno. “Spatial Dependence of Geochemical Elements in a Semiarid Agricultural Field: I. Scale Properties”. In: *Soil Science Society of America Journal* 57.5 (Sept. 1993), pp. 1316–1322. ISSN: 0361-5995, 1435-0661. DOI: 10.2136/sssaj1993.03615995005700050026x. URL: <https://access.onlinelibrary.wiley.com/doi/10.2136/sssaj1993.03615995005700050026x> (visited on 05/03/2024).
- [54] A. Gallardo. “Spatial Variability of Soil Properties in a Floodplain Forest in Northwest Spain”. In: *Ecosystems* 6.6 (2003), pp. 564–576. URL: <http://www.jstor.org/stable/3658998>.
- [55] Antonio Gallardo and Rocío Paramá. “Spatial variability of soil elements in two plant communities of NW Spain”. In: *Geoderma* 139.1 (Apr. 2007), pp. 199–208. ISSN: 00167061. DOI: 10.1016/j.geoderma.2007.01.022. URL: <https://linkinghub.elsevier.com/retrieve/pii/S0016706107000365> (visited on 11/30/2024).
- [56] K. Dana Chadwick and Gregory P. Asner. “Landscape evolution and nutrient rejuvenation reflected in Amazon forest canopy chemistry”. In: *Ecology Letters* 21.7 (July 2018). Ed. by Richard Bardgett, pp. 978–988. ISSN: 1461-023X, 1461-0248. DOI: 10.1111/ele.12963. URL: <https://onlinelibrary.wiley.com/doi/10.1111/ele.12963> (visited on 02/20/2025).

- [57] Joan E. Damerow et al. “Sample Identifiers and Metadata to Support Data Management and Reuse in Multidisciplinary Ecosystem Sciences”. In: *Data Science Journal* 20.1 (Mar. 18, 2021), p. 11. ISSN: 1683-1470. DOI: 10.5334/dsj-2021-011. URL: <https://datascience.codata.org/article/10.5334/dsj-2021-011/> (visited on 02/19/2025).

680

TOC Graphic

681



Supporting Information 1: Derivation of measurement model (Eq. 1-2)

1 Notation

- $[M]$ is solid-phase base cation elemental abundance
- $[T]$ is solid-phase immobile tracer elemental abundance
- f_s denotes feedstock endmember
- $bsln$ denotes baseline soil endmember
- $^0_{mix}$ denotes initial mixture between feedstock and baseline endmembers, *i.e.*, soil following feedstock amendment and tillage
- $_{mix}$ denotes weathered mixture, *i.e.*, following some feedstock dissolution

2 Defining f_d

The fraction of feedstock dissolved (f_d) is defined here as the complement of the fraction of feedstock remaining (f_r):

$$f_d = 1 - f_r$$

where f_r is the portion of feedstock cations still remaining in the solid-phase:

$$f_r = \frac{[M]_{mix} - [M]_{bsln}}{[M]^0_{mix} - [M]_{bsln}}$$

yielding Eq. 1 in the manuscript:

$$f_d = 1 - \frac{[M]_{mix} - [M]_{bsln}}{[M]^0_{mix} - [M]_{bsln}}$$

This formulation assumes negligible mass loss with feedstock dissolution, justified by relatively low feedstock mass fractions of 0.1-3% relative to the baseline endmember in the initial and weathered mixtures.

3 Calculating $[M]^0_{mix}$

Using an element-element mixing model with immobile tracer T , the increase in cation concentration can be calculated [1]:

$$[M]^0_{mix} - [M]_{bsln} = \frac{[M]_{fs} - [M]_{bsln}}{[T]_{fs} - [T]_{bsln}} ([T]^0_{mix} - [T]_{bsln})$$

such that assuming $[T]^0_{mix} = [T]_{mix}$ and solving for $[M]^0_{mix}$ yields Eq. 2 in the manuscript:

$$[M]^0_{mix} = [M]_{bsln} + \frac{([M]_{fs} - [M]_{bsln})([T]_{mix} - [T]_{bsln})}{[T]_{fs} - [T]_{bsln}}$$

Reference: [1] Faure, G., & Mensing, T. M. (2005). *Isotopes: Principles and Applications* (3rd ed.). Chapter 16. Hoboken, NJ: John Wiley & Sons.

Example reporting format for measurement and verification of enhanced weathering
Method: Solid-phase mass balance with element-element mixing model

Values in this example are based on a theoretical deployment;
links to relevant data could go here.

Sampling parameters:

| | | |
|--------------------------|----|-------|
| Plot area | 1 | ha |
| Compositing radius | 5 | m |
| Sub-samples per sample | 5 | cores |
| Positioning error margin | 10 | m |

Sub-samples taken along circumference at approximately equal intervals.

Target uncertainty:

| | | |
|------------------------|------------------|-----|
| Maximum relative error | ϵ_{max} | 10% |
| Minimum confidence | p_{min} | 90% |

Overall uncertainty in CDR calculation.

Target input variances:

| | | Measurement variance (ln(v)) | | |
|------------------------|--------------|------------------------------|------------|----------|
| | | Overall | Analytical | Sampling |
| Baseline cation conc. | $[M]_{bsln}$ | -6.5 | n/a | -6.5 |
| Baseline tracer conc. | $[T]_{bsln}$ | -6.5 | n/a | -6.5 |
| Mixture cation conc. | $[M]_{mix}$ | -6.5 | n/a | -6.5 |
| Mixture tracer conc. | $[T]_{mix}$ | -6.5 | n/a | -6.5 |
| Feedstock cation conc. | $[M]_{fs}$ | n/a | n/a | n/a |
| Feedstock tracer conc. | $[T]_{fs}$ | n/a | n/a | n/a |

See Steps 1-2 for determining baseline and mixture target variances, specifically Step 2.3 for calculating the values entered here.
Feedstock assumed perfectly homogeneous.
Analytical variance assumed negligible, would be subtracted from *Overall* to determine *Sampling* variances.

For spatially explicit input:

| | | Plot-scale spatial variance (ln(CV)) | | |
|-----------------------|--------------|--------------------------------------|----------|---------|
| | | Preliminary | Baseline | Mixture |
| Baseline cation conc. | $[M]_{bsln}$ | -2 | -1.8 | -1.8 |
| Baseline tracer conc. | $[T]_{bsln}$ | -3 | -3.3 | -3.3 |
| Mixture cation conc. | $[M]_{mix}$ | -2 | -1.8 | -1.9 |
| Mixture tracer conc. | $[T]_{mix}$ | -3 | -3.3 | -3.7 |
| Sample size: | | 30 | 11 | 11 |

See Steps 3-4 for determining minimum sample size, specifically Step 4.2 for calculating the *Baseline* and *Mixture* sample sizes entered here, as well as suggested sample sizes for *Preliminary* point sampling.
Plot-scale here is 1 hectare.
Dashed outline indicates where spatial variances for mixtures are assumed equal to baseline.

| | | Expected value (mg/kg) | | |
|-----------------------|--------------|------------------------|----------|---------|
| | | Preliminary | Baseline | Mixture |
| Baseline cation conc. | $[M]_{bsln}$ | 3000 | 2645 | 2645 |
| Baseline tracer conc. | $[T]_{bsln}$ | 30 | 32.12 | 32.12 |
| Mixture cation conc. | $[M]_{mix}$ | 3500 | 3142 | 3271 |
| Mixture tracer conc. | $[T]_{mix}$ | 35 | 36.11 | 34.21 |

Dashed outline indicates where mixture values are calculated using an ideal mixing model.

For other input:

| | | Expected value (mg/kg) |
|------------------------|------------|------------------------|
| feedstock cation conc. | $[M]_{fs}$ | 50,000 |
| feedstock tracer conc. | $[T]_{fs}$ | 20,000 |

Likely add another section "For temporally explicit input" for parameters with temporal variance.

Output estimates:

| | | Expected value (fraction) | |
|---|----------------|---------------------------|----------|
| | | Predicted | Measured |
| fraction of feedstock dissolved after 5 years | \hat{f}_d | 0.3 | 0.27 |
| | Maximum error: | 10% | |
| | Confidence: | 90% | |

Error and confidence will not necessarily match target uncertainty if heterogeneity estimates do not match initial estimates.